

## ARTICLE OPEN



# Seasonally distinct contributions of greenhouse gases and anthropogenic aerosols to historical changes in Arctic moisture budget

Hwa-Jin Choi<sup>1,2</sup>, Seung-Ki Min<sup>2,3✉</sup>, Sang-Wook Yeh<sup>4</sup>, Soon-Il An<sup>2,5</sup> and Baek-Min Kim<sup>6</sup>

Arctic hydrological cycle has important global implications through modifying deep ocean circulation via fresh water fluxes. However, attribution of the observed changes in Arctic moisture budget remains challenging due to the lack of reliable observations. Here, as a first step, past changes in hydrological cycle over the Arctic were evaluated using CMIP6 historical simulations. To examine possible influences of individual external forcings, CMIP6 multi-model simulations performed under natural-plus-anthropogenic (ALL), greenhouse gas (GHG), natural (NAT), and aerosol (AER) forcings were compared. Results indicate that Arctic precipitation and evaporation increase in ALL and GHG but decrease in AER. In ALL and GHG, Arctic precipitation increases in summer mainly due to enhanced poleward moisture transport whereas Arctic moistening during winter is affected more by increased surface evaporation over sea-ice retreat areas. In AER, Arctic precipitation tends to decrease due to reduced evaporation over sea-ice advance areas during cold months. Poleward meridional moisture flux (MMF) across 70°N is the strongest in summer due to the highest moisture. GHG has stronger MMF than other forcing simulations due to larger increase in moisture in line with stronger warming. The MMF response is found to be largely determined by variations in transient eddies with distinct seasonal and regional contributions.

*npj Climate and Atmospheric Science* (2023)6:189; <https://doi.org/10.1038/s41612-023-00518-9>

## INTRODUCTION

The Arctic climate system has undergone dramatic changes over the last few decades including fast warming and abrupt sea-ice melting, which can affect the Arctic hydrological cycle<sup>1</sup>. Arctic precipitation change could affect global climate by modulating the Atlantic meridional overturning circulation<sup>2</sup>. Net precipitation, river discharge, sea ice formation, and ice melt all affect the salinity distribution in the Arctic Ocean. Positive freshwater fluxes into the Arctic might lower the surface salinity and strengthen stratification, thereby decreasing deep water formation<sup>3</sup>.

In addition to greenhouse gas increases, aerosols are major factors influencing climate through direct (interaction with radiation) and indirect ways (interaction with cloud) and the aerosol-cloud interaction contributes most to their net cooling effect<sup>4</sup>. The net global cooling effect is dominated by sulfate aerosols. While greenhouse gas concentrations show steady increases, sulfate aerosols increased during 1950s–1970s and then became stabilized at global scale. This change of aerosol forcing is due to the cancellation between increased aerosol emissions from Asia and reduced aerosol emissions over North America and Europe since 1980s<sup>5</sup>. Although anthropogenic influences, mainly due to greenhouse gas increases, have been detected in the observed Arctic warming and sea-ice reduction<sup>6,7</sup> quantifying greenhouse gas and aerosol contributions to the Arctic hydrology change remains a challenge.

Previous studies have provided strong evidence for an anthropogenic contribution, which is a combined influence of greenhouse-gas and other anthropogenic forcing factors

including aerosols, to the observed changes in the Arctic: the substantial warming in Arctic land surface temperature<sup>6</sup>, the rapid decline of Arctic sea-ice<sup>7</sup> and the intensification of Arctic land precipitation<sup>8,9</sup>. Najafi et al.<sup>6</sup> demonstrated that increases in greenhouse gases have induced Arctic land warming during the past century but that global cooling effect by anthropogenic aerosols has canceled out about 60% of the greenhouse-gas-induced Arctic warming. Similarly, Mueller et al.<sup>7</sup> showed that the greenhouse gas-induced Arctic sea ice extent decrease has been offset about 23% by anthropogenic aerosol forcing during 1953–2012. However, these studies estimated aerosol influences indirectly since there were limited simulations of aerosol-only experiments.

Compared to temperature and sea-ice, Arctic hydrological cycle changes have not been extensively studied by comparing individual forcing experiments including aerosol-only runs. Stjern et al.<sup>10</sup> investigated multi-model responses of Arctic amplification and precipitation to idealized climate forcings such as a doubling of greenhouse gases and a fivefold increase in sulfate aerosols<sup>11</sup>. They found that the Arctic amplification of surface warming and Arctic precipitation increase per degree global warming are robust features among different climate forcings. In addition, Arctic precipitation responses resembled those of the Arctic warming with a maximum in winter and minimum in summer, indicating that Arctic warming is an important driver of Arctic moistening<sup>8,12</sup>. They also showed that Arctic precipitation (normalized to global warming) responses to sulfate aerosols are stronger than greenhouse gases. In this respect, analyzing single model future

<sup>1</sup>Department of Earth and Environmental Sciences, Jeonbuk National University, Jeonju, South Korea. <sup>2</sup>Division of Environmental Science and Engineering, Pohang University of Science and Technology, Pohang, South Korea. <sup>3</sup>Institute for Convergence Research and Education in Advanced Technology, Yonsei University, Incheon, South Korea. <sup>4</sup>Department of Marine Science and Convergence Engineering, Hanyang University, Ansan, South Korea. <sup>5</sup>Department of Atmospheric Sciences/Irreversible Climate Change Research Center, Yonsei University, Seoul, South Korea. <sup>6</sup>Department of Environmental Atmospheric Sciences, Pukyong National University, Busan, South Korea.

✉email: skmin@postech.ac.kr

**Table 1.** List of CMIP6 model and number of simulations used for moisture budget analysis in this study.

Model	Number of simulations	Horizontal Resolution (Vertical resolution)	Reference
BCC-CSM2-MR	1	320 × 160 (L46)	Wu et al. <sup>46</sup>
CanESM5*	10 (10*)	128 × 64 (L49)	Swart et al. <sup>47</sup>
CNRM-CM6-1*	6 (3*)	256 × 128 (L91)	Voltaire et al. <sup>48</sup>
HadGEM3-GC31-LL*	3 (3*)	192 × 144 (L85)	Roberts et al. <sup>49</sup>
IPSL-CM6A-LR*	5 (5*)	144 × 143 (L79)	Boucher et al. <sup>50</sup>
MIROC6*	3 (3*)	256 × 128 (L81)	Tatebe et al. <sup>51</sup>
MRI-ESM2-0*	3 (3*)	320 × 160 (L39)	Yukimoto et al. <sup>52</sup>
NorESM2-LM	3	144 × 96 (L32)	Seland et al. <sup>53</sup>

Asterisks (\*) indicate models and their ensemble simulations used to analyze vertically integrated meridional moisture flux.

projections, Pan et al.<sup>13</sup> showed that the solid-to-liquid precipitation transition in the Arctic is more sensitive to global aerosol reduction than increased greenhouse gas emission under the same degree of global warming, leading to more rainfall and total precipitation. Although these studies provide useful insights about the individual forcing contribution, they are based on idealized conditions with very strong forcings and thus limited to assess the past changes in Arctic hydrological cycle during the past decades.

The state-of-the-art climate models from Coupled Model Inter-comparison Project Phase 6 (CMIP6)<sup>14</sup> provide datasets from various historical simulations performed under the observed individual forcing changes during 1850–2020<sup>15</sup>. These include greenhouse gas-only (GHG), natural-only (solar and volcanic activities, NAT), and anthropogenic aerosol-only (AER) forcing simulations. Also, natural-plus-anthropogenic forcing experiment (ALL) considers all historical natural and anthropogenic forcings. See Methods for more details. There are 8 CMIP6 models that provide datasets from these individual forcing simulations, which enable one to quantify individual forcing contributions to Arctic hydrological changes for an expanded period up to 2020. In particular, better evaluation of the role of aerosol forcing is possible by using AER simulations compared to the previous studies. Further, CMIP6 models were assessed to have improved representations of sea ice extent, edge, and retreat, which are important factors driving biases in the Arctic climate<sup>16</sup>.

In this study, we investigated hydrological changes in the Arctic over the past several decades (1960–2019) using CMIP6 multi-model simulations performed under ALL, GHG, NAT, and AER forcing conditions. In particular, we examined seasonally distinct responses of hydrological components and associated meridional moisture fluxes to different forcings to have a better understanding of past changes in Arctic hydrological cycle.

## RESULTS

### Changes in Arctic moisture budget

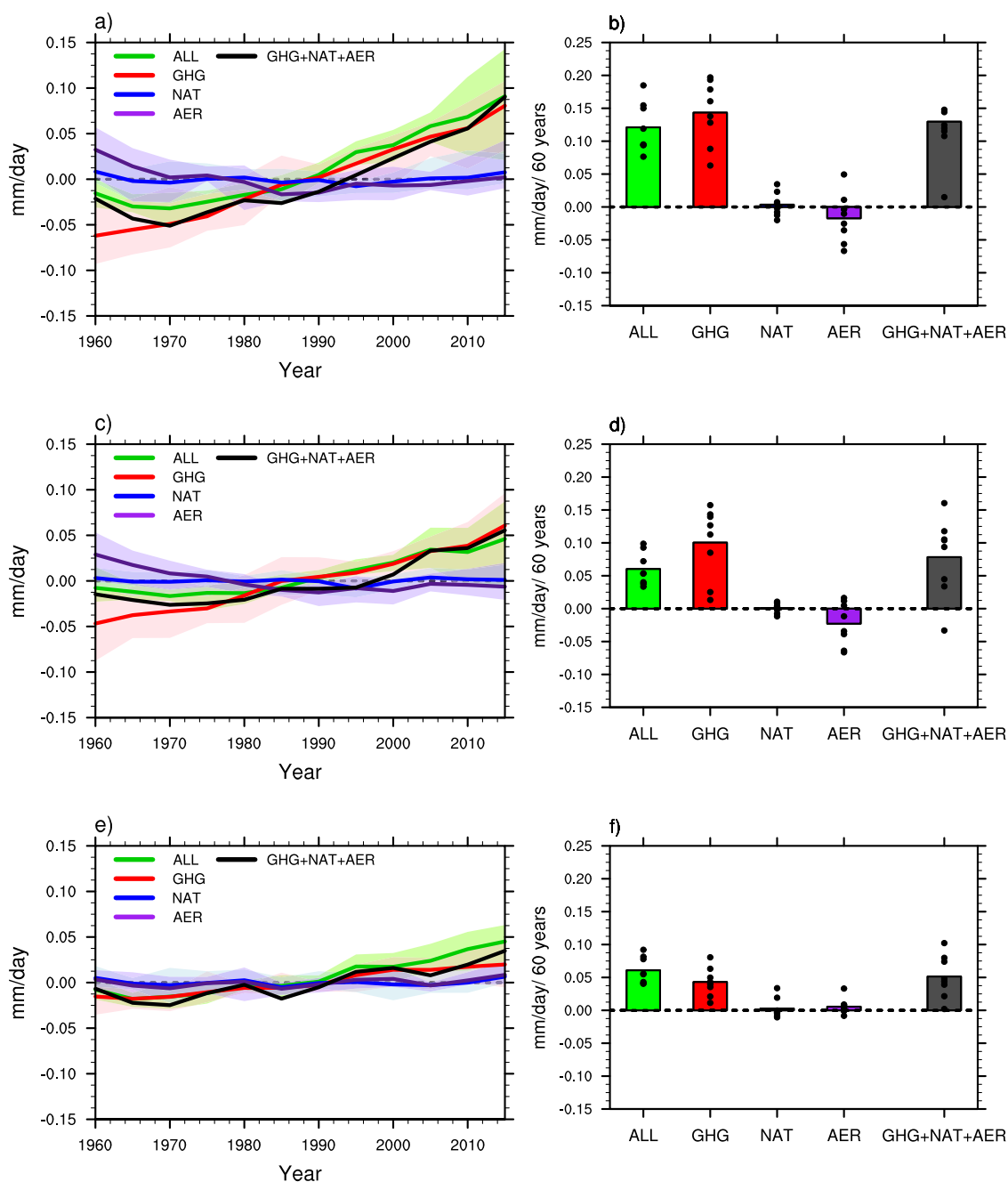
We first compare long-term trends in precipitation, evaporation, and moisture transport to the Arctic using eight CMIP6 models that provide individual forcing simulations (Table 1, see Methods for details). Figure 1a, c, and e illustrate time series of 5-year mean area-averaged anomalies of precipitation (P) and evaporation (E) over Arctic region (70°N–90°N) and net poleward moisture transport across latitude 70°N (F, estimated as P–E, see Methods) for 1960–2019 from CMIP6 multi-model means (MMEs) for different forcing experiments. Long-term trends of P, E, and F are displayed in Figs. 1b, d, and f. ALL simulations of P and E show a slight decrease during 1960s and subsequently steady and strong increases, resulting in a long-term increasing trend. These are well consistent with temperature responses (Supplementary Fig. 1), indicating a possible influence of anthropogenic aerosols during the early period<sup>6</sup>. As expected, GHG simulations of P and E

exhibit monotonic increases over the past 60 years with stronger trends than ALL, also following temperatures (Supplementary Fig. 1). In contrast, AER simulations exhibit long-term negative trends in P and E due to steady decreases until 1980s and stabilized patterns, reflecting changes in aerosol forcing and associated temperatures during the period<sup>17</sup> (Supplementary Fig. 1). ALL and GHG show F increases (Fig. 1e, f). No significant trends are found in NAT simulations, indicating negligible impacts of solar and volcanic forcing to the long-term trends in Arctic hydrology. The influence of volcanic eruptions (e.g., 1991 Mount Pinatubo) are not clearly seen even in annual time series (not shown). When comparing ALL with GHG + NAT + AER (gray lines), they exhibit overall similar variations and long-term trends, indicating the linear additivity of individual forcings in Arctic moisture budget components.

Spatial patterns of CMIP6 MME long-term trends of P, E, P–E, and sea-ice concentration (SIC) are displayed in Fig. 2. Note that P–E indicates the convergence of moisture transport at each location. Gray dots indicate poor inter-model agreement where <75% of the models (six out of eight) have the same sign of changes. ALL and GHG simulations display overall positive trends in P in the Arctic region. In northern Barents and Kara Seas, the increase in surface evaporation appears more strongly in GHG than in ALL, in accordance with stronger Arctic warming<sup>6</sup> and associated sea-ice retreat<sup>7</sup>, supporting previous results based on future simulations<sup>12</sup>. In contrast, AER exhibits counteracting decreasing trends in P and E, especially over the North Pacific Ocean, in line with the long-term Arctic cooling due to aerosol forcing and associated slight increases in SIC<sup>6,7</sup>. Stronger increases in P–E are observed over the North Pacific and North Atlantic Oceans from ALL and GHG simulations. NAT simulations exhibit no consistent long-term trends across variables. GHG + NAT + AER patterns of P, E, P–E, and SIC are similar to those of ALL, representing that external forcing influences on in Arctic moisture budget are linearly additive.

### Transport and evaporation contribution to precipitation change

In order to quantify the relative contribution of surface evaporation and poleward moisture transport changes to Arctic precipitation trends, results from monthly moisture budget analysis changes are illustrated in Fig. 3. Green asterisks (\*) indicate total Arctic precipitation changes (i.e., sum of four bars) in each month. Arctic warming (Supplementary Fig. 1) and sea-ice retreat is expected to intensify the local hydrological cycle within the Arctic region by increasing the amount of open water and amplifying surface evaporation rates<sup>12,18</sup>. We note that Arctic warming will increase atmospheric moisture amount which can lead to less sea ice through an enhanced water vapor feedback<sup>19,20</sup>. Arctic cooling caused by anthropogenic aerosol increases could also contribute



**Fig. 1** Simulated 5-year mean anomalies in Arctic precipitation, evaporation, and poleward moisture transport across 70°N and long-term trends for 1960–2019. Time series of 5-year mean area-averaged anomalies of (a) precipitation, (c) evaporation, and (e) poleward moisture transport from CMIP6 multi-model simulations with anthropogenic plus natural (ALL, green), only greenhouse gas (GHG, red), anthropogenic aerosol (AER, purple), natural forcing (NAT, blue) over Arctic region (70°–90°N) during 1960–2019. The summed results of GHG, NAT and AER (GHG + NAT + AER, gray) are also displayed. Shadings indicate inter-model ranges for each experiment. Long-term trends in (b) precipitation (P), (d) evaporation (E), and (f) poleward moisture transport ( $F = P - E$ ). Black dots indicate individual model values.

to sea ice extent increase as shown above (see SIC response to AER in Fig. 2). This indicates that sea-ice extent is an important contributor to evaporation rates by enlarging or reducing open waters. Therefore, we defined three sub-regions (sea-ice retreat region, sea-ice advance region, and sea-ice non-related region) of the Arctic and examined region-averaged changes in evaporation (see Methods for details).

The simulated Arctic precipitation over 1960–2019 varies across simulations. ALL and GHG simulate general increases in Arctic precipitation changes (Fig. 3a, b). In contrast, in AER, overall decreases in precipitation are observed (Fig. 3d). Seasonally, Arctic

precipitation increases peak in late autumn and winter in ALL and GHG simulations, during which Arctic precipitation decreases peak in AER. The winter peak of Arctic precipitation changes was found in future projections and attributed to surface evaporation changes through the seasonal ocean heat storage/release and other ice-related climate feedbacks<sup>12</sup>.

The relative contribution of E and F to precipitation changes significantly varies according to seasons and individual forcing experiments (different color bars in Fig. 3). ALL and GHG simulations show similar seasonal variations of E and F (Figs. 3a, 3b), which resembles future projections forced by stronger GHG forcing<sup>12</sup>. In

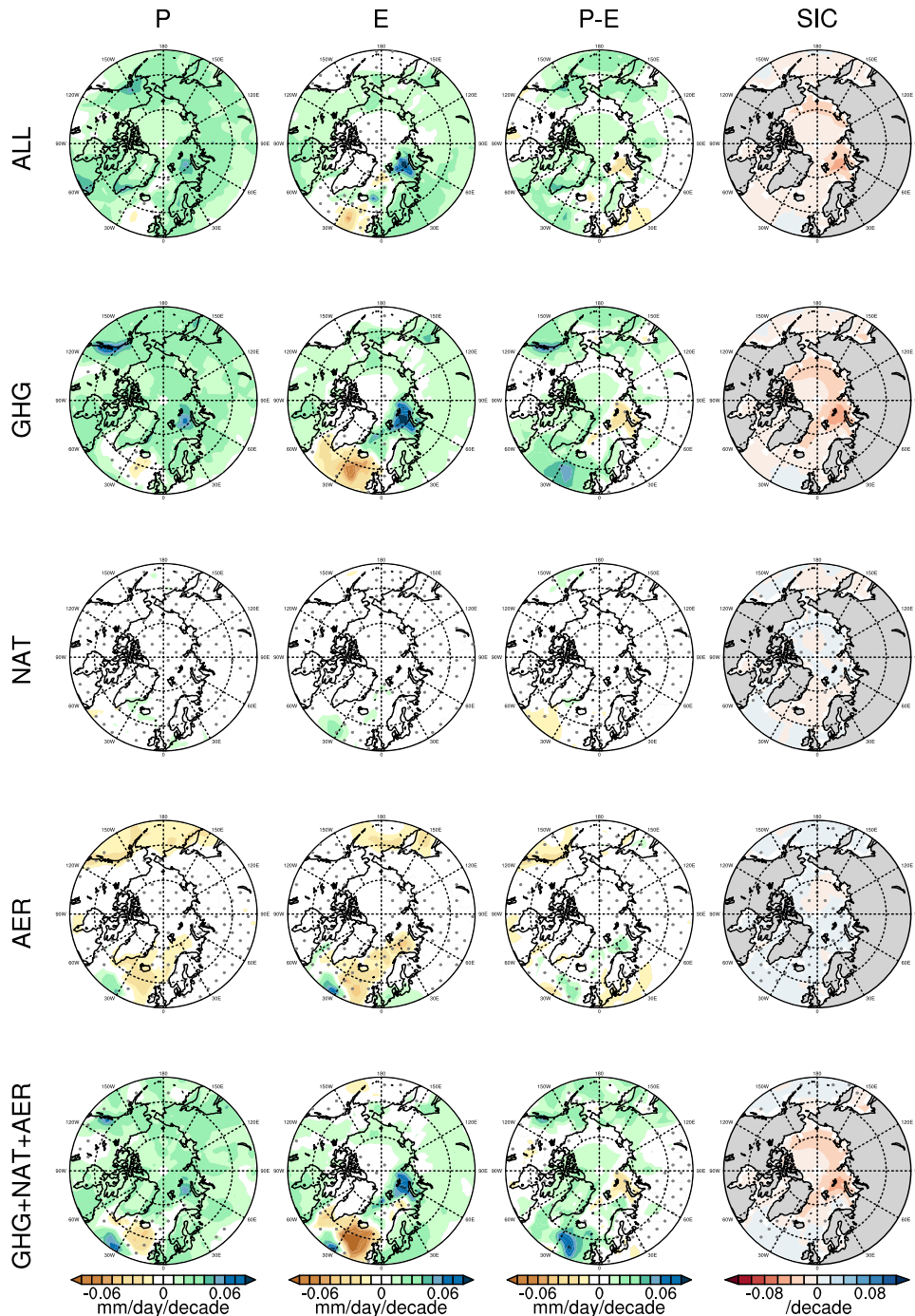


**Fig. 2** Geographic distribution of long-term trends in precipitation, evaporation, moisture transport convergence, and sea-ice cover in the Arctic region. Spatial patterns of long-term trends in precipitation (P) evaporation (E) convergence of moisture transport (P–E) and sea-ice concentration (SIC) during 1960–2019 from CMIP6 multi-model simulations with ALL, GHG, NAT, and AER. GHG + NAT + AER patterns are also displayed for comparison. Gray dots show regions of low inter-model agreement where <75% (six out of eight) have the same sign of trends.

both experiments, moisture transport changes peak in summer and autumn when north-south moisture gradient increases most strongly following warming<sup>3,21</sup> (i.e. thermodynamics). The poleward moisture flux in summer explains 92 and 75% of precipitation changes in ALL and GHG, respectively. In late autumn and winter, in contrast, enhanced surface evaporation plays an important role in contributing to the increases in Arctic precipitation, accounting for 77 and 89% of the precipitation increase in ALL and GHG, respectively. Especially, the proportion of sea-ice retreat to the total Arctic evaporative change is as large as 59% in ALL and 66% in

GHG, which is supported by spatial patterns of E trends, exhibiting strong increases along marginal ice zones (see below for further discussion). As expected from stronger sea-ice melting (Fig. 2), the evaporation contribution due to sea-ice retreat is stronger in GHG than in ALL during late autumn to winter. NAT simulations generally exhibit only small changes in all components (Fig. 3c). In AER, overall decreasing trend of Arctic precipitation is attributed to reduced evaporation caused by sea-ice advance. Changes over sea-ice advance regions account for 70% of total evaporation changes in AER (Fig. 3d).

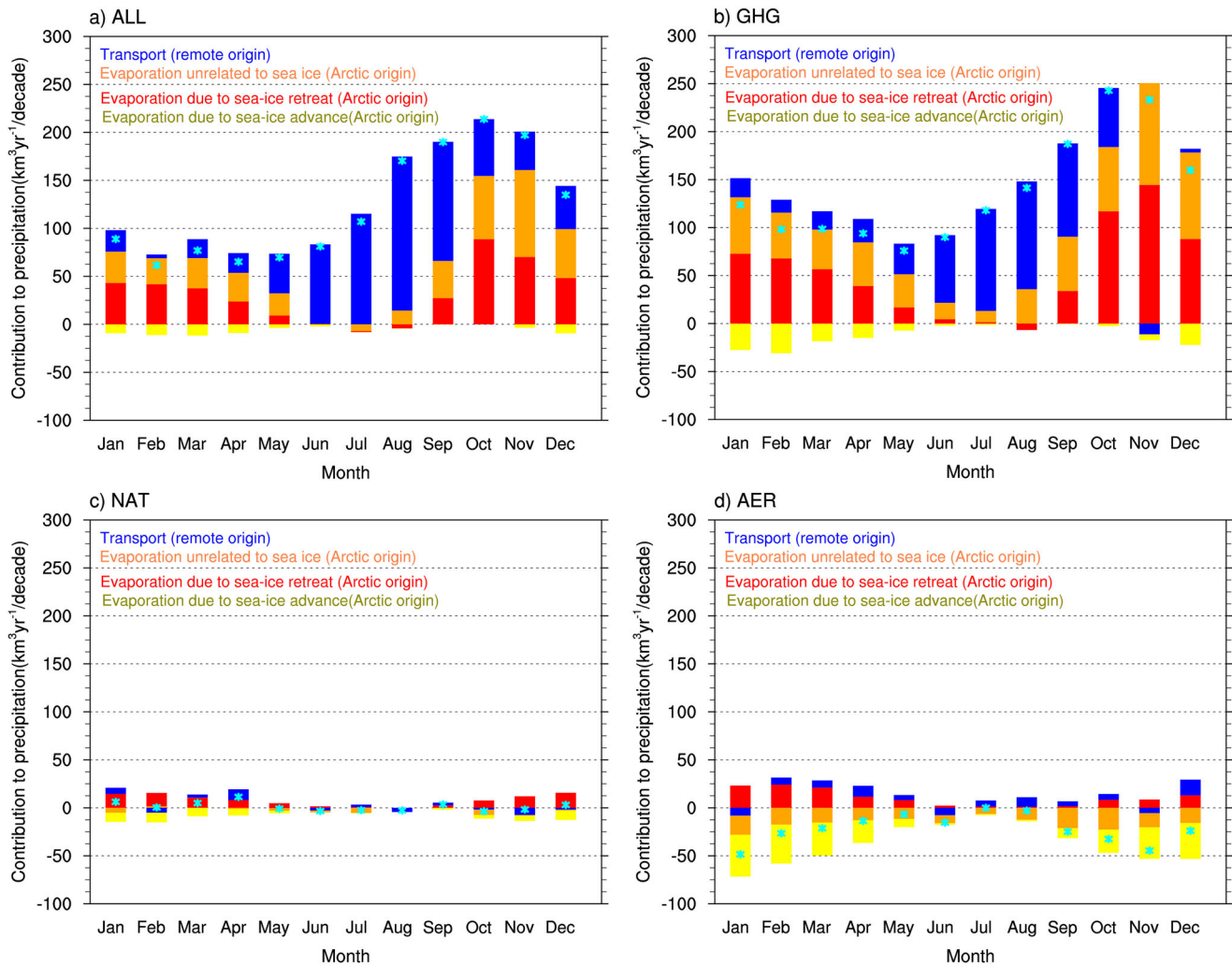


**Fig. 3** Monthly changes in poleward moisture transport across 70°N and surface evaporation components during 1960–2019. Results for (a) ALL, (b) GHG, (c) NAT, and (d) AER. Each bar represents the monthly and multi-model mean. Total Arctic surface evaporation is separated into ice-retreat (red), ice-advance (yellow), and sea ice non-related (orange) components. Cyan asterisks (\*) indicate net Arctic precipitation changes (i.e., sum of four bars).

### Moisture transport to the Arctic

The vertically integrated meridional moisture flux (MMF) can be divided into contributions of mean meridional circulation (MMC), stationary eddies (SE), and transient eddies (TE)<sup>22,23</sup>. SE represents moisture transport due to deviations of specific humidity and northward wind from the zonal mean, whereas TE represents deviations from the temporal mean, i.e., synoptic fluctuations<sup>24</sup>. We analyze poleward MMF and its components across 70°N by integrating moisture flux through an atmospheric column (see Methods for details). Note that six models that provide daily datasets are used (Table 1). Supplementary Figure 2 illustrates annual means of zonally averaged MMF, MMC, SE and TE for 1960–2019. MMF is the sum of MMC, SE, and TE in each latitude. MMC is related to the Polar cell, which extends from the pole to 60°N~70°N. Air in the Polar cell sinks over high latitudes and flows out towards lower latitudes at the surface. The role of SE in poleward moisture transport is weaker than that of TE, consistent with a reanalysis-based assessment<sup>23</sup>, supporting that TE plays an important role in poleward moisture transport in high latitude.

Long-term trends in zonal averaged MMF, MMC, SE, and TE from ALL, GHG, NAT, and AER runs are compared as shown in Fig. 4. MMF, SE, and TE tend to increase overall in ALL and GHG. At 70°N, the contribution of moisture transport components to the increase

in MMF is slightly different between ALL and GHG. In ALL, the change of TE is responsible for most (109%) of the MMF change at 70°N, whereas contributions of MMC and SE are −32 and 23%, respectively. In GHG, contributions of TE, MMC, and SE are 69, −19, and 50%, respectively, indicating an increased importance of SE. Note that the negative trend in MMC corresponds to an increasing contribution to MMF since MMC produces equatorward fluxes. Monthly averages of poleward MMFs across 70°N are analyzed (Supplementary Fig. 3). Temporal and spatial distributions of atmospheric moisture are associated with air temperatures through the Clausius-Clapeyron relationship, i.e. warmer air can hold more water vapor. Thus, the MMF is the highest in summer due to a lot of moisture. The poleward MMF is stronger in GHG than in other simulations while AER shows weaker MMF and TE than other forcings (Supplementary Fig. 3). The difference in MMF across different forcings is well linked to their difference in surface temperatures (Supplementary Fig. 4a). Due to the temperature dependence of moisture amount, the increasing trends in specific humidity are strongest in ALL and GHG during summer and early autumn (Supplementary Fig. 4b), consistent with reanalysis-based results<sup>3</sup>.

Monthly changes of vertically integrated MMFs across 70°N are presented in Fig. 5, where asterisks denote that at least five out of

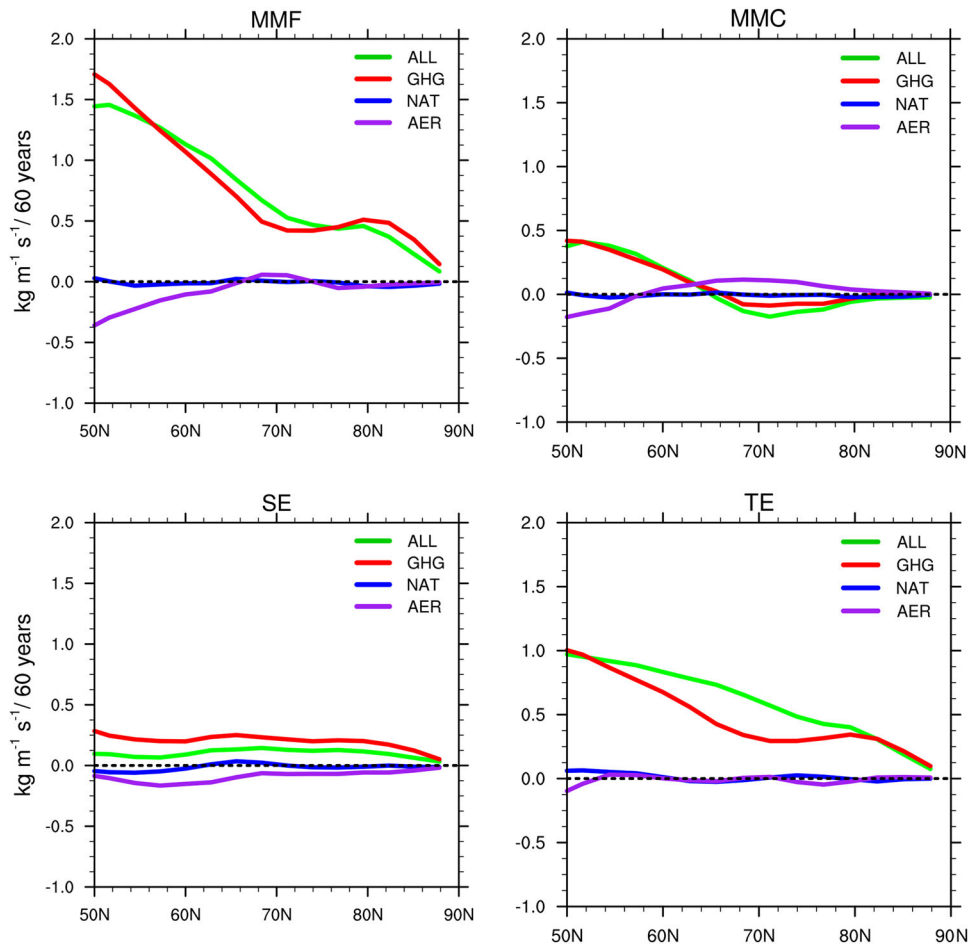


**Fig. 4** Long-term trends of zonally averaged meridional moisture flux (MMF), mean meridional circulation (MMC), stationary eddies (SEs), and transient eddies (TEs) for 1960–2019. MMF is the sum of MMC, SE, and TE in each latitude. Green, red, blue, and purple line represent ALL, GHG, NAT, and AER simulations, respectively.

six models have the same sign of changes, indicating good inter-model agreement. Simulated trends of moisture transport to the Arctic are positive in ALL and GHG simulations for most months. In summer, the contribution of MMF components to MMF changes varies with month. The change of MMF in GHG is the highest in August because TE change has a maximum value, explaining 58% of the MMF change. Summer SE shows overall positive increases but with smaller amplitudes (around 25% of MMF change). In TE changes, ALL is greater than GHG for all seasons.

Relations between changes in Arctic precipitation and changes in the MMF, MMC, SE and TE transports across 70°N are further examined using an inter-experiment correlation analysis (Fig. 6). GHG and ALL results are generally located close to each other with larger amplitudes compared to NAT and AER. This results in statistically significant linear relationships between Arctic precipitation change and changes of MMF, SE and TE. The MMF change and Arctic precipitation change are significantly correlated across all CMIP6 experiments ( $r = 0.81$ ) at 1% level. Precipitation shows significant positive inter-forcing correlations with SE ( $r = 0.80$ ) and TE ( $r = 0.80$ ). This indicates that model simulations with stronger changes (usually GHG and ALL) in MMF, SE, and TE tend to have stronger changes in precipitation and vice versa.

#### MMFs in Pacific and Atlantic sectors

Figure 7 shows spatial patterns of seasonal trends in the poleward MMF for different forcing experiments. Trends of MMF in the Arctic vary considerably across regions. Iceland and Norway have

a large variability of MMF in the Atlantic sector. Overall, summer and autumn possess stronger trends in the Arctic region than winter and spring. GHG runs show stronger trends than other forcings. Although ALL and GHG differ in the intensity of trends, their regional patterns are quite similar. The MMF in the Norwegian Sea increases strongly in all seasons. In contrast, Alaska and Northeastern Russia (120°W–120°E) in the Pacific sector have different responses according to individual forcings. In this region, there is a difference between GHG and AER, evident in autumn and winter. The poleward MMF in AER decreases in Alaska but increases in Northeastern Russia. On the contrary, in GHG simulations, the poleward MMF increases in Alaska but decreases in Northeastern Russia during autumn and winter. Supplementary Figure 5 shows spatial patterns of seasonal trends in TE. Trend amplitudes in ALL and GHG are larger than in NAT and AER. In summer, ALL and GHG share increases in TE over the Beaufort Sea (160°W–120°W). Regional trends in summer TE across 70°N (Supplementary Fig. 6) show a greater increase in ALL than GHG over western Eurasia (0°–90°E), which could partly explain a greater contribution of Atlantic sector to the change of TE in ALL than in GHG during summer. GHG + NAT + AER result shows a very similar behavior to ALL, indicating that TE responses to different forcings are largely additive. This also suggests contributions of NAT and AER to the TE increases over western Eurasia. Spatial patterns of seasonal MMF trends in NAT and AER show much weaker trends with limited regions having good inter-model agreement (Fig. 7), in line with the large uncertainty in Arctic averaged trends (Fig. 1).

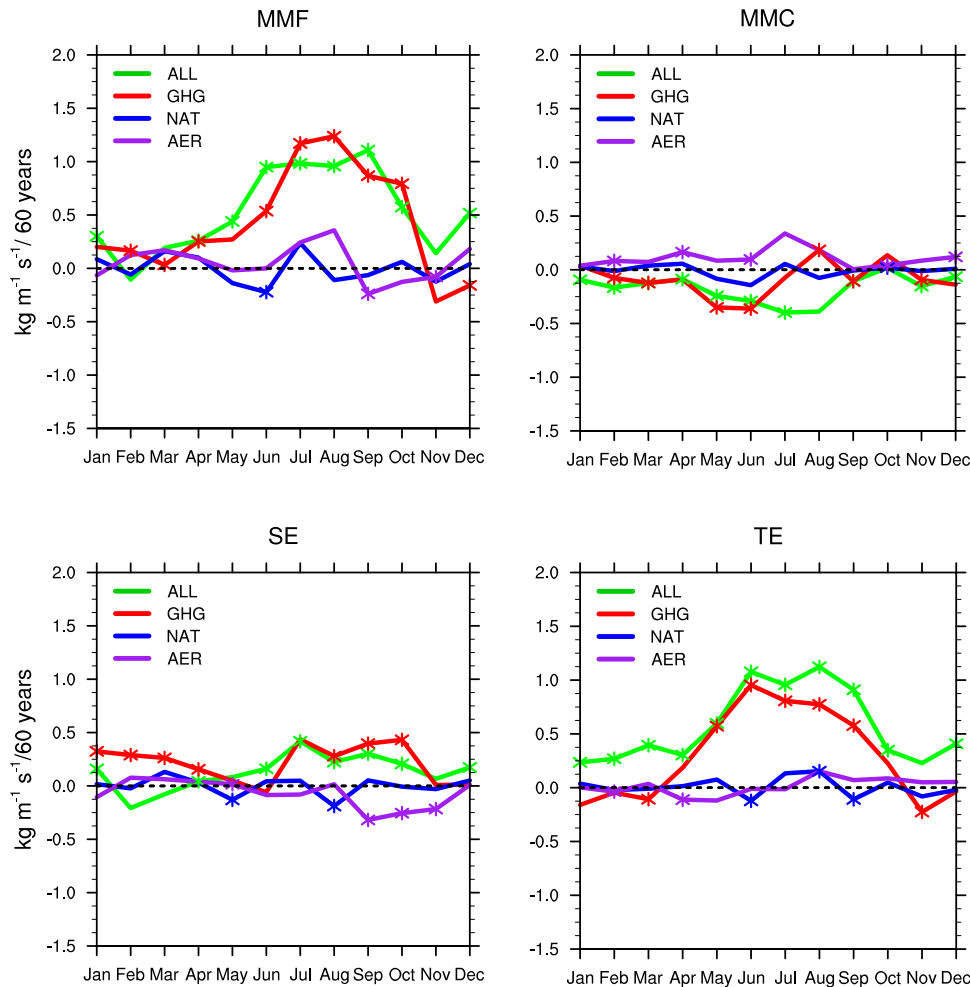


**Fig. 5** Monthly trends of MMF, MMC, SE, and TE across 70°N during 1960–2019. MMF is divided into contributions of MMC, SE, and TE. Asterisks indicate that at least five out of six models have the same sign.

To explore regional patterns of SE and TE trends during 1960–2019, MMF trends across 70°N are separated into two components from the Pacific (90°E to 90°W) and Atlantic (90°W to 90°E) sectors (see Methods). Figure 8 shows distributions of regional contributions to total TE trends. ALL and GHG have similar seasonal variations of TE changes with greater Pacific contribution during summer. However, regional contributions to the MMF differ considerably between experiments. In ALL, TE increase in Pacific sector is stronger (explaining 60% of total change) than that of Atlantic sector during summer. However, Atlantic contribution becomes dominant during autumn (explaining 78%). GHG exhibits weaker contribution of Atlantic during summer than ALL. Trends during winter are characterized by a negative contribution from Atlantic sector, suggesting a large uncertainty in TE trends over the Atlantic Ocean<sup>3</sup>. No distinct patterns of TE trends are observed in NAT and AER. The SE across 70°N in ALL and GHG increases overall in all months but with much weaker amplitudes than TE (Supplementary Fig. 7). The largest increases in SE appear in July, with more contribution from the Pacific sector. In short, there are different regional contributions to the total MMF, depending on seasons as well as experiments. Detailed mechanism controlling these regional responses is beyond the scope of this study and warrants further investigation.

## DISCUSSIONS

Although moisture budget analysis helps to identify moisture sources for additional precipitation, increased moisture availability

is necessary but not sufficient to cause precipitation<sup>25,26</sup>. This means that in addition to atmospheric water vapor, the process which condensates moisture (adiabatic cooling due to updrafts) is needed for formation of precipitation and that the updrafts are closely linked to large scale dynamics in the Arctic. Recently, Pithan and Jung<sup>27</sup> found relatively low sensitivity of boreal winter moisture availability (based on precipitable water) to surface warming over the Arctic and proposed that Arctic winter precipitation increase might be rather energetically driven by enhanced atmospheric radiative cooling. In this respect, we have checked the moisture sensitivity to surface warming over the Arctic region (70°N–90°N) using CMIP6 GHG simulations (Supplementary Table 1). During boreal winter (DJF), precipitable water (PW) is found to increase by 4.6% per degree of surface warming, which is slightly larger than the precipitation sensitivity (3.8% K<sup>-1</sup>). Annual means show similar rates (4.8 and 4.1% K<sup>-1</sup> for PW and precipitation, respectively) while summer (JJA) means exhibit stronger sensitivity (10.2 and 6.2% K<sup>-1</sup>, respectively). The smaller impact of warming on precipitable water in winter than in summer is associated with the seasonally different responses in surface warming and moisture increase. The strong Arctic amplification in winter occurs due to stable stratification while Arctic surface warming is suppressed by sea ice during summer<sup>19,28</sup>. Summer surface warming is weakened due to the large effective heat capacity of melting ice. In addition, the cold surface temperature with strong inversions during winter induces a positive lapse-rate feedback, enhancing surface-trapped

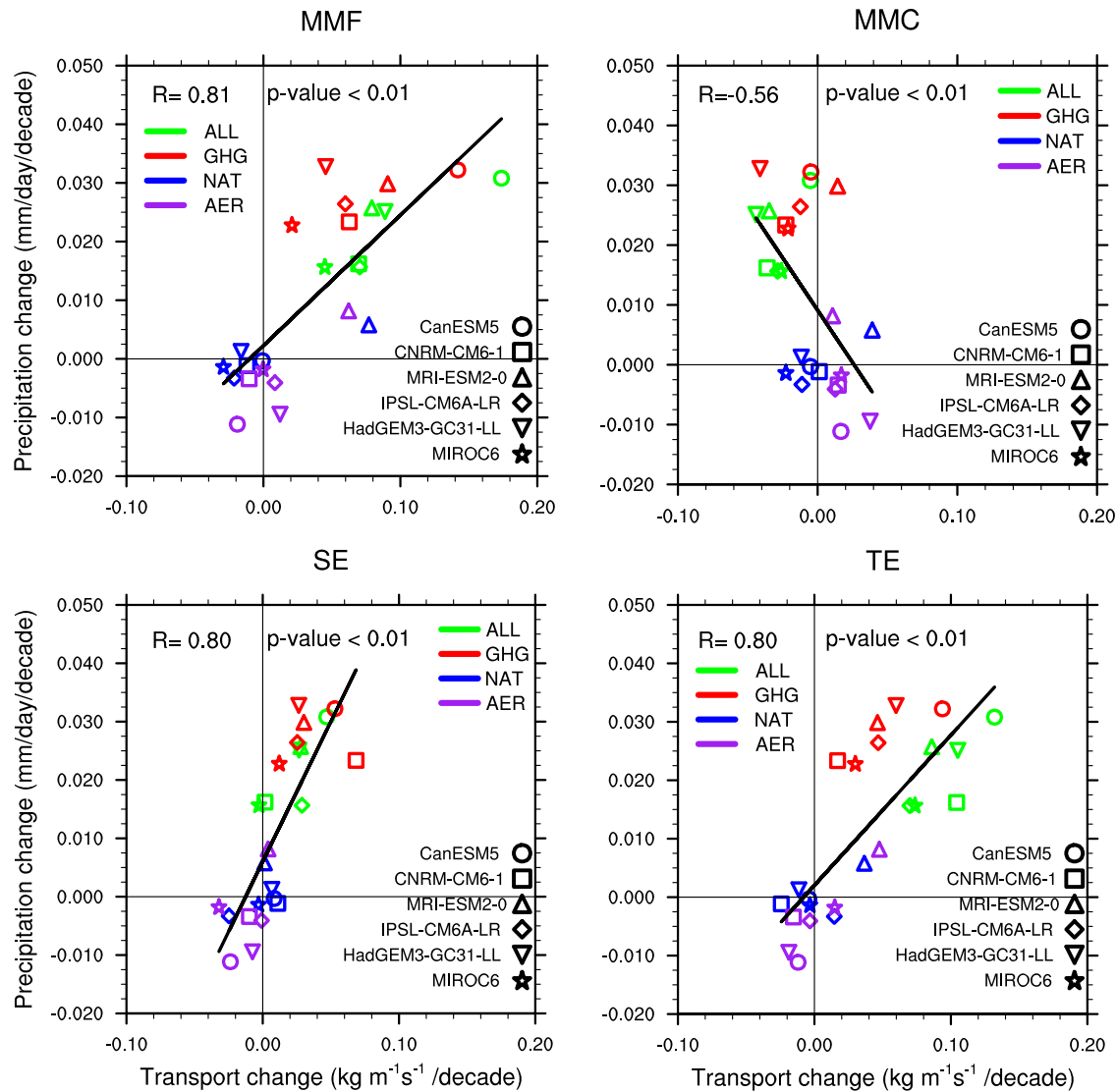


**Fig. 6** Relations between Arctic precipitation change and meridional moisture flux and its components. Scatter plots showing inter-model relations between changes in precipitation (70–90°N average) and MMF and its components (across 70°N). Linear regression line and correlation coefficients with corresponding  $p$ -values based on all 24 models (black) are presented.

warming<sup>28</sup>. Although temperature increase is smaller during summer than winter, moisture increases are relatively large in summer than winter (Supplementary Table 1). Our analysis (Fig. 3) indicates that the larger moisture increases in summer than in winter is due to the increased poleward moisture transport. This simple evaluation suggests the important role of moisture availability in Arctic precipitation sensitivity in our models even during winter, differing from Pithan and Jung<sup>27</sup>. This discrepancy might be due to different periods (historical vs. long-term future) and/or methods (Arctic mean vs. zonal mean precipitable water). The  $4.6\% \text{ K}^{-1}$  scaling in the Arctic we found from historical GHG simulations matches previous estimates based on future simulations. In particular, Bintanja and Selten<sup>12</sup> concluded that the sensitivity of Arctic mean precipitation ( $4.5\% \text{ K}^{-1}$ ) is much larger than the global mean value ( $1.6$  to  $1.9\% \text{ K}^{-1}$ ). They emphasized that the relatively high sensitivity of Arctic precipitation compared to other regions is mainly due to the presence of sea ice, whose melting under warming provides moisture through enhanced surface evaporation. Our study confirms the important role of the increased evaporation and moisture transport from lower latitudes in the Arctic moistening in the historical period and also demonstrates that the opposite response of evaporation occurs

to the aerosol forcing. Understanding historical responses of Arctic hydrology to individual forcing has important implications for attributing observed changes given the large observational uncertainty. Although main focus of this study is to examine Arctic moisture budget responses to individual forcing during the historical period, detailed physical processes explaining the interlinkage of water and energy budgets in the Arctic needs to be further investigated.

Since we are considering averaged moisture budget within the Arctic region, precipitation will increase in proportion to increased evaporation and/or moisture transport by definition<sup>3</sup>. This supports our findings that both moisture transport and local evaporation contributes to the atmospheric moisture and thereby precipitation. Although Arctic mean moisture budget shows the important contribution of evaporation to precipitation, it is an important question whether additional evaporation at the Arctic surface indeed fuels precipitation within the Arctic. We have checked this by evaluating the relationship between E and MMF. Analyzing ERA5 reanalysis for 1979–2018, Nygård et al.<sup>29</sup> found that increased evaporation intensifies moisture transport in the sea ice margin (positive correlation between E and MMF) while, in the open sea such as the area south of Greenland, moisture



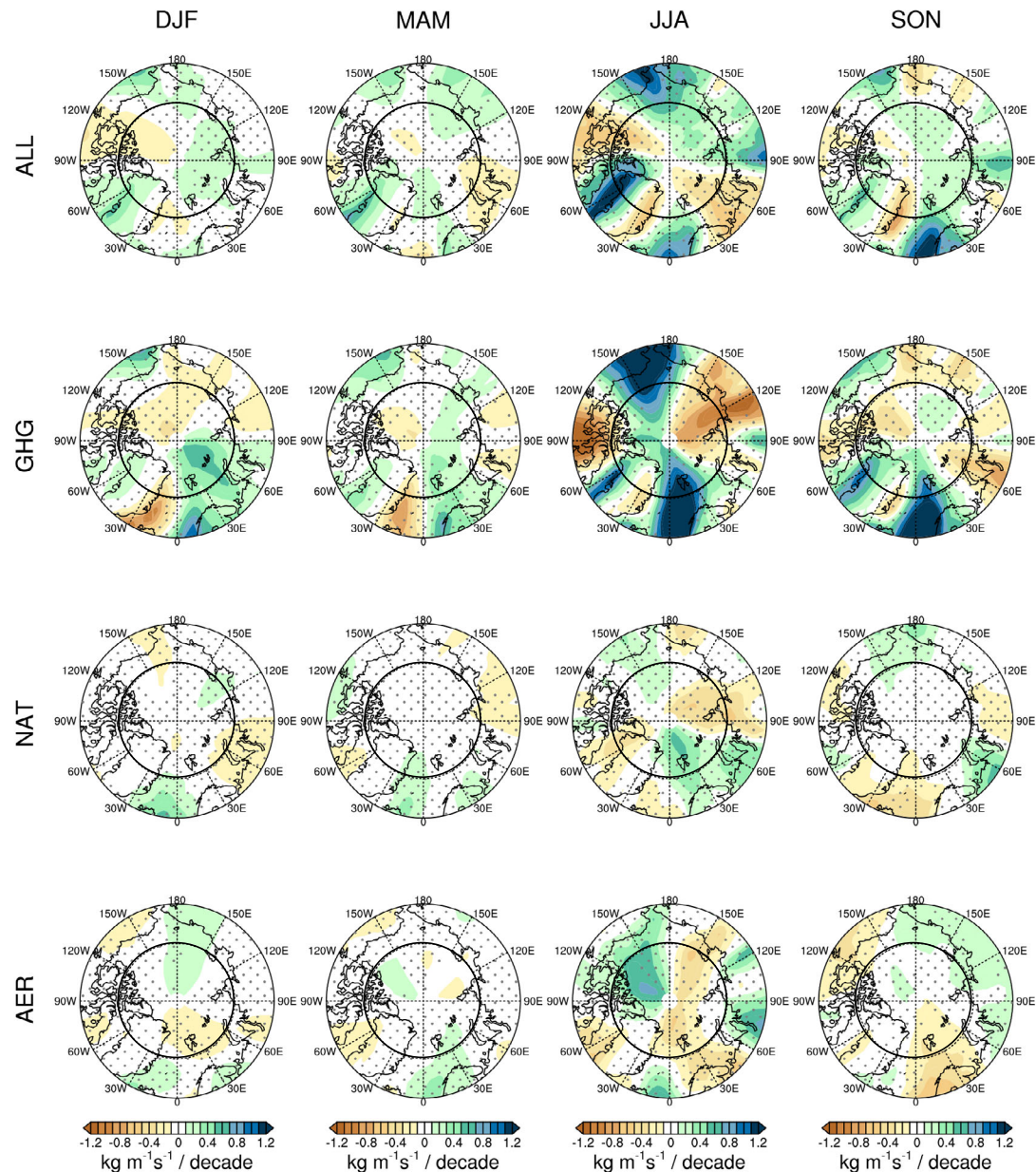


**Fig. 7** Spatial patterns of seasonal changes in MMF during 1960–2019. Gray dots indicate areas of low inter-model agreement where <75% of the models (five out of six) have the same sign. Black line depicts 70°N.

transport tends to suppress evaporation (negative correlation) by decreasing the humidity difference between the surface and the air above, which was observed consistently during cold season. We have examined whether the same E-MMF correlation holds in our CMIP6 simulations. Using ALL, GHG, NAT, and AER runs for 1960–2019, we have calculated correlation maps between E and MMF during DJF (Supplementary Fig. 8). Corresponding trend maps of E and MMF are also displayed for comparison. Interestingly, all simulations exhibit a positive correlation over the Arctic region (70°N–90°N) and a negative correlation in the open sea regions, largely consistent with Nygård et al.<sup>29</sup>. This supports that, at the marginal ice zone where sea ice melting is strong, moisture transport and local evaporation have the same contribution to the atmospheric moisture and thereby precipitation. E and MMF in the sea-ice margin have the same signs of trends (positive in ALL and GHG and negative in AER). However, contribution of enhanced evaporation for precipitation in the

Arctic might not be very large as a lot of moisture evaporated in the Arctic can be transported southwards. The inverse relation between E and MMF in the open sea area further from sea ice boundary, particularly, south of Greenland is supported by the opposite trends between them in ALL, GHG and AER runs, suggesting that MMF induces the opposite direction of change in E by modifying the air-surface humidity difference, as discussed in Nygård et al.<sup>29</sup>.

It should be noted that the correlations do not indicate causal relationships between evaporation and moisture transport but that correlations are dependent on which processes are important. Also, these correlations are based on interannual variations, calculated from annual DJF means following Nygard et al.<sup>29</sup>, and in this time scale the moisture transport (often connected with heat transport) could increase evaporation by causing sea ice melt. Quantifying the import and export of moisture through the Arctic is important to specify the associated moisture pathways<sup>30</sup> but is

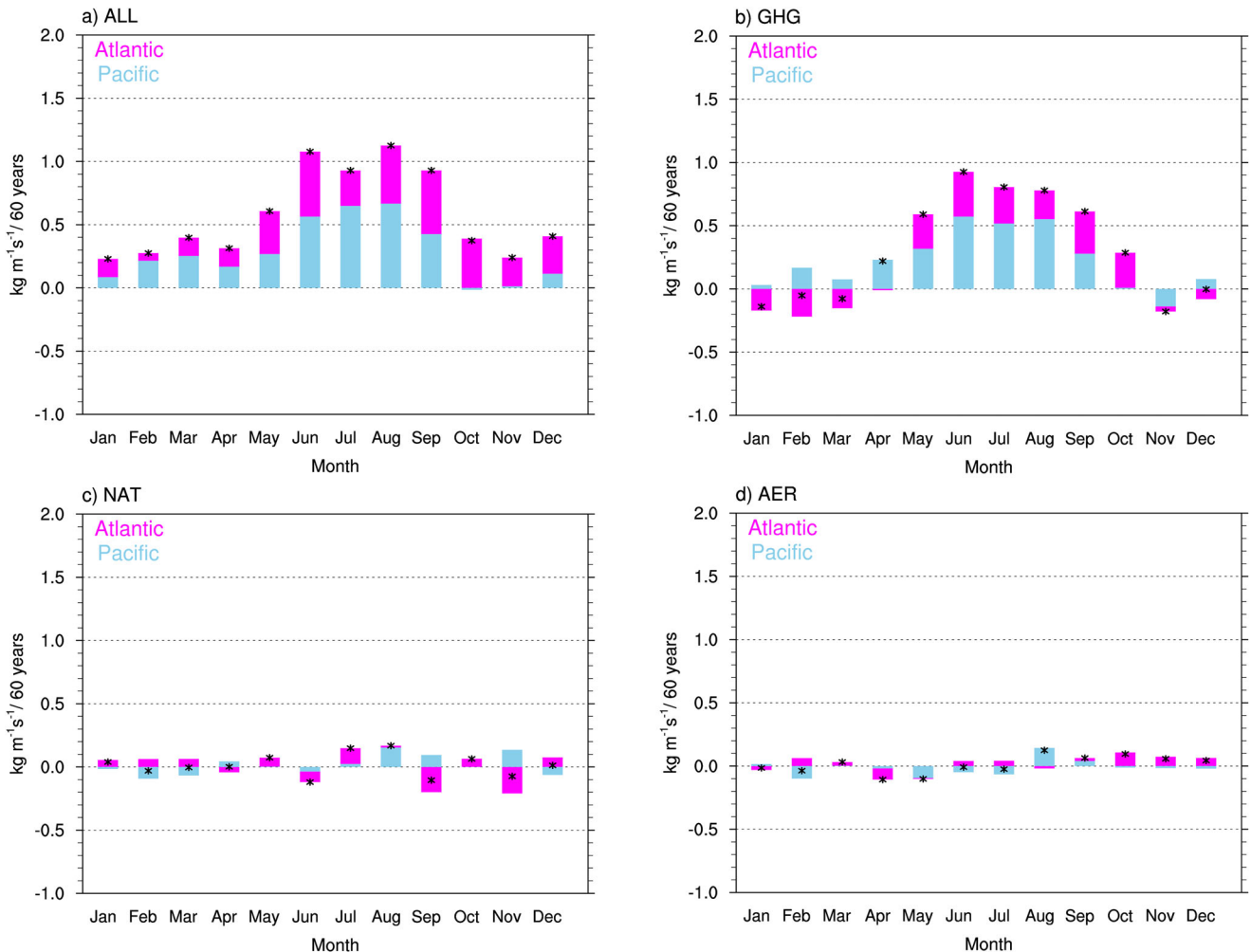


**Fig. 8** Trends in monthly TE across 70°N in the Pacific sector and Atlantic sector during 1960–2019. Results for (a) ALL, (b) GHG, (c) NAT, and (d) AER. TE is separated into that of Atlantic sector (magenta) and Pacific sector (light blue). Black asterisks (\*) indicate total TE changes across 70°N, which are the sum of two sectors in each month.

outside of the scope of this study which focuses on overall Arctic moisture budget responses to different forcings. In this respect, natural variability like North Atlantic Oscillation can affect the long-term trend in moisture exchange through the Arctic particularly during cold season<sup>21,31,32</sup>. Further details about regional-scale responses and feedback processes affecting the Arctic hydrology need to be explored in a separate study.

Although a few reanalysis data have covered a long-term period for the analysis of Arctic moisture budget, there are still substantial differences in their trends amplitudes, particularly for atmospheric moisture transport and evaporation, among different reanalyses, indicating large uncertainties<sup>18,29,33,34</sup>. Using available five reanalyses (JRA55, ERA5, NCEP1, 20CRv2c, and ERA-20C; see Supplementary Table 2), we have compared their time series of P, E, and F during 1960–2019 with CMIP6 ALL results (Supplementary Fig. 9). Note that 20CRv2 (1960–2014) and ERA-20C (1960–2009) cover shorter periods. Results show that P increases in all reanalyses with trends ranging from 0.01–0.022 mm day<sup>-1</sup> decade<sup>-1</sup>. One recent study<sup>35</sup> found no significant trend in Arctic Ocean precipitation but they used different reanalyses and considered a larger domain of Arctic Ocean and a shorter period (1979–2019) than our case. This difference indicates the important influence of reanalysis datasets and spatiotemporal coverages when assessing long-term trends in P. E shows a consistent increase but with a larger difference in trend amplitudes among reanalysis with a

minimum (0.003 mm day<sup>-1</sup> decade<sup>-1</sup>) in 20CRv2 and a maximum (0.025 mm day<sup>-1</sup> decade<sup>-1</sup>) in JRA55. ERA5 shows comparable trends between P and E (~0.02 mm day<sup>-1</sup> decade<sup>-1</sup>), which is consistent with the estimates of Ford and Frauenfeld<sup>36</sup>. Due to the large cross-reanalysis differences in E trends, long-term trends in F, which is estimated as P-E, are diverse across reanalyses even with different signs (negative in JRA55, near zero in ERA5 and NCEP1, and positive in 20CRv2 and ERA-20C). This indicates that large uncertainties remain in Arctic moisture budgets and trends in reanalyses, supporting previous studies<sup>34,36</sup> who pointed out the evaporation trend as one of the important factors driving the inter-reanalysis differences. Further, evaluation of moisture transport using P-E might be inaccurate in reanalyses since assimilation of observations can affect atmospheric water vapor content irrespective of atmospheric moisture balance. Other uncertainty factors include changes in atmospheric circulation, sea surface temperature, sea ice cover, and total cloud cover as well as assimilation methods and data used.

Reliable observations based on satellite and remote sensing datasets are also limited to estimate observed long-term trends in precipitation and moisture in the Arctic. The primary reasons for insufficient satellite datasets in the Arctic include the short temporal coverage and the lack of spatially well-covered data. It is only in the 1990s that satellite remote sensing using microwave has begun to give significant information on air moisture and

**Table 2.** Information about variables used in moisture budget analysis and vertically integrated meridional moisture flux analysis.

	Moisture budget analysis	Vertically integrated meridional moisture flux
Analysis period	1960–2019	1960–2019
Frequency	Monthly	Daily
Vertical level	Surface	1000, 850, 700, 500, 250 (hPa)
Variables	Precipitation, 2 m air temperature, surface upward latent heat flux	Specific humidity, northward wind, surface pressure

clouds<sup>37</sup>. The records of ground-based remote sensing measurements are short as well, and there are only a few stations in the circumpolar Arctic that perform these measurements of humidity and cloud properties<sup>38,39</sup>. In addition, the satellite-borne precipitation sensors (e.g., Global Precipitation Measurement Mission) only cover an area of around 65°N<sup>40</sup>.

MMF can be underestimated due to relatively coarse vertical resolution and time interval<sup>41</sup>. A quantitative comparison of the uncertainty related to time resolution using available CMIP6 models could be useful. However, CMIP6 models analyzed in this study provide daily outputs at the five pressure levels only. Instead, here we have tested the sensitivity of MMF calculations to the temporal and vertical resolution using JRA55 reanalysis. The climatology of zonal mean MMF and its components (MMC, SE, and TE) across 70°N is calculated for three cases and results are compared (Supplementary Table 3): (1) five vertical levels and daily output, (2) five vertical levels and 6 hourly output, and (3) 21 vertical levels and daily output. Compared to 6 hourly data, daily output is found to lead to underestimation of MMF (~11%), which is dominated by TE, supporting the finding of Seager and Henderson<sup>41</sup>. Results also show that MMF can be underestimated due to the coarse vertical resolution. When increasing vertical resolution from 5 levels (3 levels below 700 hPa) to 21 levels (11 levels below 700 hPa), MMF becomes stronger by ~10%, which is contributed by the strengthened TE and SE and the weakened MMC. This implies a large uncertainty in MMF calculations caused by vertical resolutions particularly at lower troposphere. Assuming that errors associated with these temporal and vertical resolutions are systematic (i.e. not changing much as time), their influences on MMF trends may not be strong. Nevertheless, our sensitivity analysis suggests that temporally and vertically high-resolution data are required for correct estimates of MMF. A systematic comparison using CMIP6 models that provide 6 hourly data at all pressure levels (Table 1) would be useful to assess if the use of high vertical resolution reduces the uncertainty in MMF.

It still remains challenging to attribute the observed changes in Arctic hydroclimate to human influences due to the lack of long-term reliable observations<sup>33,34,36</sup>. Considering this limitation, the present study utilized CMIP6 historical simulations and examined past changes in Arctic moisture budget during 1960–2019 under different external forcing factors. Key components of moisture budget were identified for different seasons, including meridional moisture flux (MMF). In particular, this study isolated greenhouse (GHG) and aerosol (AER) contributions to changes of atmospheric moisture budget over Arctic and its subregions.

Using external forcing simulations, we evaluated long-term changes in precipitation, evaporation, and poleward moisture transport. Results show that evaporation and precipitation increase in ALL (natural-plus-anthropogenic) and GHG simulations but decrease in AER. Results from spatial patterns of long-term trends indicate that precipitation generally increases over the Arctic in ALL and GHG. Evaporation increases are also strong over sea-ice retreat regions. They are stronger in GHG than in ALL, supporting previous results based on future simulations<sup>12</sup>. Atmosphere moisture in the Arctic can be explained by local evaporation and poleward moisture transport. In ALL and GHG, increases of Arctic precipitation in summer are attributed to

enhanced poleward moisture inflow while increases in winter are due to intensified local surface evaporation in sea-ice retreat regions. In AER, Arctic precipitation tends to decrease during cold season due to reduced evaporation over sea-ice advance regions. Results from monthly trends of MMF and its components show that in summer and early autumn, transient eddy (TE) is a main driver of the increased poleward moisture transport with weaker contributions from stationary eddy and mean meridional circulation changes in ALL and GHG.

Our results demonstrate that long-term trends of MMF according to individual forcings vary by region. Causes for such differences need to be explored<sup>3</sup>. Especially, the increase of TE is greater in ALL than in GHG in summer due to the greater contribution of the Atlantic sector, particularly western Eurasia, than the Pacific in ALL. There might be contributions of NAT and AER but further investigation is warranted to explore possible mechanisms for such distinct regional contributions. Relative contributions of north-south moisture gradient and atmospheric circulation changes including the North Atlantic Oscillation<sup>32</sup>, which are known to be important at multi-decadal and inter-annual time scales<sup>18,21,42</sup>, need to be examined in the future study.

## METHODS

### CMIP6 simulation data

Historical changes in atmospheric moisture budget over the Arctic during 1960–2019 were investigated using multi-model datasets from CMIP6 individual forcing experiments<sup>15</sup>. Here the Arctic is defined as the area 70°N–90°N following previous studies<sup>12,23,36</sup>, which corresponds to the Arctic Ocean where sea-ice and precipitation changes are dominant. When using 65°N, results are not affected much (not shown). We used historical (ALL) simulations performed with the observed anthropogenic (greenhouse gases and anthropogenic aerosols) and natural (solar and volcanic activities) external forcings for 1960 to 2014. ALL simulations were extended up to 2019 using corresponding SSP2-4.5 scenario runs. To explore the influence of individual external forcings, we used greenhouse-gas-only (hist-GHG; GHG), natural forcing (hist-nat; NAT), and aerosol-only (hist-aer; AER) simulations for 1960–2019. As explained in the introduction, global aerosol forcing is characterized by a steady decrease during 1950s–1980s followed by stabilization due to the large cancellation between different regions. We used eight CMIP6 models which provide data for all forced simulations (Table 1). Different models have different number of ensemble members (total 34 runs), and to give equal weight to individual models, we calculated ensemble means of individual models first and then obtained the multi-model mean using them. This way can, however, make some differences in each model's variability (i.e. more reduced variability in models having larger ensemble size). When testing sensitivity to the use of a single ensemble member from each model, multi-model means and inter-model agreement remain largely unaffected (not shown).

Monthly data from eight models were used to analyze the Arctic moisture budget (Table 2). Total evaporation was computed from latent heat flux since CMIP6 multi-models do not provide total evaporation (see below). To calculate vertically integrated

meridional moisture flux, daily data from six models (27 runs) were used. These data included specific humidity, northward wind component, and surface pressure (Table 2). Vertical integrations were conducted using five identical levels (1000, 850, 700, 500 and 250 hPa; CMIP6 standard pressure levels). Note that the lower bound of vertical integration is the surface pressure (see below for details).

### Computation of evaporation

Evaporation is the process of a liquid becoming vaporized. Energy absorbed during evaporation can be transformed from latent heat flux, which is given in an energy flux form<sup>43,44</sup>. The relation between surface evaporation  $E$  (unit: mm day<sup>-1</sup>) and latent heat flux  $LH$  (unit: W m<sup>-2</sup>) is shown below:

$$E = \frac{LH}{L_e} \quad (1)$$

where  $L_e$  is the latent heat of evaporation (J kg<sup>-1</sup>), which can be approximated with the following:

$$L_e \approx 2.501 \times 10^6 - 2370T_c \quad (2)$$

where  $T_c$  is the near-surface temperature in Celsius. Calculations of  $E$  using Eqs. (1) and (2) were done in daily time scales and then monthly and seasonal means were obtained using daily estimates. We note that  $LH$  calculated in climate models considers latent heat of sublimation as well as latent heat of evaporation. As the latent heat for sublimation is about 12% larger than that for evaporation<sup>45</sup>, this means that  $E$  calculated based on  $L_e$  can be overestimated accordingly over snow and ice surfaces. However, considering that Arctic mean  $E$  response to external forcing is dominated by the ocean region with sea-ice retreat or sea-ice advance (Fig. 2), main results are unlikely to be affected much.

### Moisture budget analysis

Atmosphere moisture in the Arctic is a result of local evaporation and moisture transport from lower latitudes<sup>3</sup>. A moisture budget analysis of the Arctic has been introduced by Bintanja and Selten<sup>12</sup> to examine relative contributions of poleward moisture transport and surface evaporation components to Arctic precipitation. Long-term moisture budget of the Arctic atmosphere can be expressed as  $\frac{\partial Q}{\partial t} = F - (P - E)$ , where  $Q$  is the total moisture content of the atmosphere,  $P$  is the total Arctic precipitation (downward),  $F$  is the poleward atmospheric moisture transport across 70°N, and  $E$  is the Arctic surface evaporation (positive upward). The Arctic atmospheric moisture reservoir is considerably small, meaning that  $\frac{\partial Q}{\partial t} \ll F, P, E$ . Therefore, we can evaluate contributions of moisture transport and local evaporation to the Arctic precipitation using the balance of  $P = F + E$ <sup>12</sup>.

Arctic sea-ice plays an important role in surface evaporation rate. As sea-ice declines, the amount of open water increases and surface evaporation amplifies, and vice versa. Therefore, to assess the contribution of evaporation accurately, we divided the Arctic region into sea-ice retreat region, sea-ice advance region, and sea-ice non-related region following Bintanja and Selten<sup>12</sup>. We compare sea-ice concentration (SIC) between early decade (1960–1969) and recent decade (2010–2019), which is equivalent to assessing long-term trends. Relative to the 1960–1969 mean condition, grids with large decrease in SIC are classified into ‘sea-ice retreat’ region while areas with large increase in SIC belong to ‘sea-ice advance’ region. Specifically, sea-ice retreat region was defined as the region where mean values of SIC for 2010–2019 were <50% (currently small sea-ice) and fractional changes in SIC from 1960–1969 to 2010–2019 were less than -30% (considerable decrease from the past). Sea-ice advance region was specified by the area where mean SIC values for 2010–2019 were >50% (currently large sea-ice) and fractional changes in SIC were more than +30% (considerable increase from the past). We defined

areas where neither of them occurred as sea-ice non-related region (see Supplementary Fig. 10 for an example). We also calculated each model ensemble mean of evaporation changes for the three defined regions and then obtained multi-model means. We tested sensitivity of our results to the use of slightly different thresholds for sea-ice concentrations and found that our main results were overall unaffected.

### Vertically integrated meridional moisture flux

To calculate poleward MMF across 70°N, integrations through an atmospheric column were made from surface pressure to 250 hPa. Surface pressure data were used to define lower boundary for vertical integral. Taking a vertical integral of daily northward wind component and specific humidity through an atmospheric column, we have the following equation:

$$MMF = -\frac{1}{g} \int_{P_s}^{250hPa} qv dp \quad (3)$$

The vertically integrated MMF (kg m<sup>-1</sup> s<sup>-1</sup>) can be decomposed into contributions of mean meridional circulation (MMC), stationary eddies (SEs), and transient eddies (TEs) applying Reynolds decomposition<sup>23,24</sup>:

$$MMF = -\frac{1}{g} \int_{P_s}^{250hPa} [\bar{q}][\bar{v}] dp - \frac{1}{g} \int_{P_s}^{250hPa} [\bar{q}'\bar{v}'] dp - \frac{1}{g} \int_{P_s}^{250hPa} [\bar{q}'v'] dp \quad (4)$$

where the first, second, and third terms on the right-hand side are moisture flux due to MMC, SEs, and TEs, respectively. The overbar represents temporal averaging. The square brackets denote zonal averaging. The prime and star indicate deviations from the temporal mean and zonal mean, respectively. Monthly averages were used as the temporal mean<sup>23</sup>.

### Regional contribution to MMF

The calculated MMF cannot be used to explain regional difference because vertical integration is made after zonal mean is taken when applying Reynolds decomposition. To analyze regional contributions to moisture transport, we take zonal mean after vertical integration:

$$MMF_{mod} = \left[ \int \bar{q}\bar{v} dp \right] \quad (5)$$

This modified MMF ( $MMF_{mod}$ ) is not exactly the same as the MMF since the order of the zonal mean and vertical integration is switched. Differences due to this procedure were found to be very small (<5% of original MMF value). Therefore, except for MMC, for which the order of calculation cannot be changed, two eddy terms become as follows:

$$SE_{mod} = \left[ \int \bar{q}'\bar{v}' dp \right] = SE_{Pacific} + SE_{Atlantic} \quad (6)$$

$$TE_{mod} = \left[ \int \bar{q}'v' dp \right] = TE_{Pacific} + TE_{Atlantic} \quad (7)$$

$SE_{mod}$  and  $TE_{mod}$  components can be divided into contributions from Pacific and Atlantic regions, which can be calculated as follows:

$$SE_{Region} = -\frac{1}{g} \int_{lon1}^{lon2} \left( \int_{P_s}^{250hPa} \bar{q}'\bar{v}' dp \right) dlon / \int_{0^\circ}^{360^\circ} dlon \quad (8)$$

$$TE_{Region} = -\frac{1}{g} \int_{lon1}^{lon2} \left( \int_{P_s}^{250hPa} \bar{q}'v' dp \right) dlon / \int_{0^\circ}^{360^\circ} dlon \quad (9)$$

where the Pacific sector is defined as 90°E (lon1) to 90°W (lon2) and the Atlantic sector is defined as 90°W (lon1) to 90°E (lon2).

## DATA AVAILABILITY

CMIP6 data are available at <https://esgf-node.llnl.gov/projects/cmip6/>.

## CODE AVAILABILITY

The source codes for this study are available from the authors upon reasonable request.

Received: 25 February 2023; Accepted: 1 November 2023;

Published online: 15 November 2023

## REFERENCES

- Prowse, T. et al. Arctic freshwater synthesis: summary of key emerging issues. *J. Geophys. Res. Biogeosci.* **120**, 1887–1893 (2015).
- Yang, Q. et al. Recent increases in Arctic freshwater flux affects Labrador Sea convection and Atlantic overturning circulation. *Nat. Commun.* **7**, 10525 (2016).
- Vihma, T. et al. The atmospheric role in the Arctic water cycle: A review on processes, past and future changes, and their impacts. *J. Geophys. Res. Biogeosci.* **121**, 586–620 (2016).
- Forster, P. et al. In *Climate Change 2021: The physical Science Basis. Contribution of Working Group I to the Sixth Assessment Report of the Intergovernmental Panel on Climate Change*. 1st edn, Vol. 2 (Cambridge University Press, Cambridge, USA) Ch. 923–1054 (2021).
- Aas, W. et al. Global and regional trends of atmospheric sulfur. *Sci. Rep.* **9**, 953 (2019).
- Najafi, M. R., Zwiers, F. W. & Gillett, N. P. Attribution of Arctic temperature change to greenhouse-gas and aerosol influences. *Nat. Clim. Chang.* **5**, 246–249 (2015).
- Mueller, B. L., Gillett, N. P., Monahan, A. H. & Zwiers, F. W. Attribution of Arctic sea ice decline from 1953 to 2012 to influences from natural, greenhouse gas, and anthropogenic aerosol forcing. *J. Clim.* **31**, 7771–7787 (2018).
- Min, S. K., Zhang, X. & Zwiers, F. Human-induced Arctic moistening. *Science* **320**, 518–520 (2008).
- Wan, H., Zhang, X., Zwiers, F. & Min, S. K. Attributing northern high-latitude precipitation change over the period 1966–2005 to human influence. *Clim. Dyn.* **45**, 1713–1726 (2015).
- Stjern, C. W. et al. Arctic amplification response to individual climate drivers. *J. Geophys. Res. Atmos.* **124**, 6698–6717 (2019).
- Myhre, G. et al. PDRMIP: A precipitation driver and response model inter-comparison project-protocol and preliminary results. *Bull. Am. Meteorol. Soc.* **98**, 1185–1198 (2017).
- Bintanja, R. & Selten, F. M. Future increases in Arctic precipitation linked to local evaporation and sea-ice retreat. *Nature* **509**, 479–482 (2014).
- Pan, S. et al. Larger sensitivity of Arctic precipitation phase to aerosol than Greenhouse gas forcing. *Geophys. Res. Lett.* **47**, 23 (2020).
- Eyring, V. et al. Overview of the Coupled Model Intercomparison Project Phase 6 (CMIP6) experimental design and organization. *Geosci. Model Dev.* **9**, 1937–1958 (2016).
- Gillett, N. P. et al. The Detection and Attribution Model Intercomparison Project (DAMIP v1.0) contribution to CMIP6. *Geosci. Model Dev.* **9**, 3685–3697 (2016).
- Davy, R. & Outten, S. The Arctic surface climate in CMIP6: status and developments since CMIP5. *J. Clim.* **33**, 8047–8068 (2020).
- Tokarska, K. B. et al. Past warming trend constrains future warming in CMIP6 models. *Sci. Adv.* **6**, eaaz9549 (2020).
- Serreze, M. C., Barrett, A. P. & Stroeve, J. Recent changes in tropospheric water vapor over the Arctic as assessed from radiosondes and atmospheric reanalyses. *J. Geophys. Res. Atmos.* **117**, D10104 (2012).
- Pithan, F. & Mauritsen, T. Arctic amplification dominated by temperature feedbacks in contemporary climate models. *Nat. Geosci.* **7**, 181–184 (2014).
- Goosse, H. et al. Quantifying climate feedbacks in polar regions. *Nat. Commun.* **9**, 1919 (2018).
- Skific, N., Francis, J. A. & Cassano, J. J. Attribution of projected changes in atmospheric moisture transport in the Arctic: A self-organizing map perspective. *J. Clim.* **22**, 4135–4153 (2009).
- Palmen, E. & Worela, L. A. On the mean meridional circulations in the northern hemisphere during the winter season. *Quart. J. Roy. Meteorol. Soc.* **89**, 131–138 (1963).
- Jakobson, E. & Vihma, T. Atmospheric moisture budget in the Arctic based on the ERA-40 reanalysis. *Int. J. Climatol.* **30**, 2175–2194 (2010).
- Naakka, T., Nygård, T., Vihma, T., Sedlar, J. & Graversen, R. Atmospheric moisture transport between mid-latitudes and the Arctic: regional, seasonal and vertical distributions. *Int. J. Climatol.* **39**, 2862–2879 (2019).
- Trenberth, K. E. Changes in precipitation with climate change. *Clim. Res.* **47**, 123–138 (2011).
- Pendergrass, A. G. & Hartmann, D. L. The atmospheric energy constraint on global-mean precipitation change. *J. Clim.* **27**, 757–768 (2014).
- Pithan, F. & Jung, T. Arctic amplification of precipitation changes—the energy hypothesis. *Geophys. Res. Lett.* **48**, e2021GL094977 (2021).
- Hahn, L. C., Armour, K. C., Battisti, D. S., Eisenman, I. & Bitz, C. M. Seasonality in Arctic warming driven by sea ice effective heat capacity. *J. Clim.* **35**, 1629–1642 (2022).
- Nygård, T., Naakka, T. & Vihma, T. Horizontal moisture transport dominates the regional moistening patterns in the Arctic. *J. Clim.* **33**, 6793–6807 (2020).
- Papritz, L., Hauswirth, D. & Hartmuth, K. Moisture origin, transport pathways, and driving processes of intense wintertime moisture transport into the Arctic. *Wea. Clim. Dyn.* **3**, 1–20 (2022).
- Boer, G. J., Fourest, S. & Yu, B. The signature of the annular modes in the moisture budget. *J. Clim.* **14**, 3655–3665 (2001).
- Dorn, W., Dethloff, K., Rinke, A. & Roeckner, E. Competition of NAO regime changes and increasing greenhouse gases and aerosols with respect to Arctic climate projections. *Clim. Dyn.* **21**, 447–458 (2003).
- Dufour, A., Zolina, O. & Gulev, S. K. Atmospheric moisture transport to the arctic: assessment of reanalyses and analysis of transport components. *J. Clim.* **29**, 5061–5081 (2016).
- Rinke, A. et al. Trends of vertically integrated water vapor over the Arctic during 1979–2016: consistent moistening all over? *J. Clim.* **32**, 6097–6116 (2019).
- Barrett, A. P., Stroeve, J. C. & Serreze, M. C. Arctic Ocean precipitation from atmospheric reanalyses and comparisons with North pole drifting station records. *J. Geophys. Res. Oceans* **125**, e2019JC015415 (2020).
- Ford, V. L. & Frauenfeld, O. W. Arctic precipitation recycling and hydrologic budget changes in response to sea ice loss. *Glob. Planet. Change* **209**, 103752 (2022).
- Bobylev, L. P., Zabolotskikh, E. V., Mitnik, L. M. & Mitnik, M. L. Atmospheric water vapor and cloud liquid water retrieval over the arctic ocean using satellite passive microwave sensing. *IEEE Trans. Geosci. Remote Sens.* **48**, 283–294 (2010).
- Shupe, M. D. Clouds at arctic atmospheric observatories. Part II: thermodynamic phase characteristics. *J. Appl. Meteorol. Climatol.* **50**, 645–661 (2011).
- Shupe, M. D. et al. Clouds at Arctic atmospheric observatories. Part I: occurrence and macrophysical properties. *J. Appl. Meteorol. Climatol.* **50**, 626–644 (2011).
- Hou, A. Y. et al. The global precipitation measurement mission. *Bull. Am. Meteorol. Soc.* **95**, 701–722 (2014).
- Seager, R. & Henderson, N. Diagnostic computation of moisture budgets in the ERA-interim reanalysis with reference to analysis of CMIP-archived atmospheric model data. *J. Clim.* **26**, 7876–7901 (2013).
- Sorteberg, A. & Walsh, J. E. Seasonal cyclone variability at 70°N and its impact on moisture transport into the Arctic. *Tellus A Dyn. Meteorol. Oceanogr.* **60**, 570–586 (2008).
- Lorenz, C. & Kunstmann, H. The hydrological cycle in three state-of-the-art reanalyses: Intercomparison and performance analysis. *J. Hydrometeorol.* **13**, 1397–1420 (2012).
- Su, T., Feng, G., Zhou, J. & Ye, M. The response of actual evaporation to global warming in China based on six reanalysis datasets. *Int. J. Climatol.* **35**, 3238–3248 (2015).
- Froyland, H. K., Untersteiner, N., Town, M. S. & Warren, S. G. Evaporation from Arctic sea ice in summer during the International Geophysical Year, 1957–1958. *J. Geophys. Res. Atmos.* **115**, D15104 (2010).
- Wu, T. et al. BCC-CSM2-HR: A high-resolution version of the Beijing climate center climate system model. *Geosci. Model Dev.* **14**, 2977–3006 (2021).
- Swart, N. C. et al. The Canadian Earth System Model version 5 (CanESM5.0.3). *Geosci. Model Dev.* **12**, 4823–4873 (2019).
- Voldoire, A. et al. Evaluation of CMIP6 DECK experiments With CNRM-CM6-1. *J. Adv. Model. Earth Syst.* **11**, 2177–2213 (2019).
- Roberts, M. J. et al. Description of the resolution hierarchy of the global coupled HadGEM3-GC3.1 model as used in CMIP6 HighResMIP experiments. *Geosci. Model Dev.* **12**, 4999–5028 (2019).
- Boucher, O. et al. Presentation and evaluation of the IPSL-CM6A-LR climate model. *J. Adv. Model. Earth Syst.* **12**, e2019MS002010 (2020).
- Tatebe, H. et al. Description and basic evaluation of simulated mean state, internal variability, and climate sensitivity in MIROC6. *Geosci. Model Dev.* **12**, 2727–2765 (2019).
- Yukimoto, S. et al. The meteorological research institute Earth system model version 2.0, MRI-ESM2.0: Description and basic evaluation of the physical component. *J. Meteorol. Soc. Jpn.* **97**, 931–965 (2019).
- Seland, Ø. et al. Overview of the Norwegian Earth System Model (NorESM2) and key climate response of CMIP6 DECK, historical, and scenario simulations. *Geosci. Model Dev.* **13**, 6165–6200 (2020).

## ACKNOWLEDGEMENTS

This study was supported by a National Research Foundation of Korea (NRF) grant funded by the Korean government (MSIT) (NRF-2018R1A5A1024958 and NRF-2021R1A2C3007366) and the Human Resource Program for Sustainable Environment in the 4th Industrial Revolution Society. We acknowledge the World Climate Research Programme, which, through its Working Group on Coupled Modeling, coordinated and promoted CMIP6. We thank the climate modeling groups for producing and making available their model output, the Earth System Grid Federation (ESGF) for archiving the data and providing access (<https://esgf-node.llnl.gov/projects/cmip6/>), and the multiple funding agencies who support CMIP6 and ESGF.

## AUTHOR CONTRIBUTIONS

S.-K.M. conceived the study. H.-J.C. and S.-K.M. conducted the analysis and S.-W.Y., S.-I.A., and B.-M.K. contributed to the interpretation of the results. H.-J.C. prepared the initial manuscript and all authors contributed to the manuscript writing.

## COMPETING INTERESTS

The authors declare no competing interests.

## ADDITIONAL INFORMATION

**Supplementary information** The online version contains supplementary material available at <https://doi.org/10.1038/s41612-023-00518-9>.

**Correspondence** and requests for materials should be addressed to Seung-Ki Min.

**Reprints and permission information** is available at <http://www.nature.com/reprints>

**Publisher's note** Springer Nature remains neutral with regard to jurisdictional claims in published maps and institutional affiliations.



**Open Access** This article is licensed under a Creative Commons Attribution 4.0 International License, which permits use, sharing, adaptation, distribution and reproduction in any medium or format, as long as you give appropriate credit to the original author(s) and the source, provide a link to the Creative Commons license, and indicate if changes were made. The images or other third party material in this article are included in the article's Creative Commons license, unless indicated otherwise in a credit line to the material. If material is not included in the article's Creative Commons license and your intended use is not permitted by statutory regulation or exceeds the permitted use, you will need to obtain permission directly from the copyright holder. To view a copy of this license, visit <http://creativecommons.org/licenses/by/4.0/>.

© The Author(s) 2023